Isothermal Crystallization Kinetics and Melting Behavior of Poly(oxyethylene)-*b*-poly(oxybutylene)/Poly(oxybutylene) Blends

Jun-Ting Xu,† J. Patrick A. Fairclough, Shao-Min Mai, and Anthony J. Ryan*

The Polymer Centre, Department of Chemistry, University of Sheffield, Sheffield S3 7HF, UK

Chiraporn Chaibundit‡

Department of Chemistry, The University of Manchester, Manchester M13 9PL, UK

Received March 18, 2002

ABSTRACT: Poly(oxyethylene-*b*-oxybutylene) block copolymers of various chain lengths (E_mB_n) were blended with poly(oxybutylene) homopolymer (B_h), materials having different segregation strengths and morphologies (lamellae, cylinder, and sphere) were obtained. The isothermal crystallization kinetics and melting behavior of the blends were studied using differential scanning calorimetry (DSC) and synchrotron small-angle X-ray scattering (SAXS), respectively. Two types of crystallization are identified: confined crystallization occurring at lower temperature with Avrami exponent close to 1.0, having a strong dependence of crystallization halftime on crystallization temperature and a smooth change of q^* in crystallization; breakout crystallization occurring at higher temperature with an Avrami exponent much bigger than 1.0 and a step change in q^*. The relative segregation strength χ_c/χ_{ODT} has an important influence on the crystallization mechanism, and confined crystallization is observed at $\chi_c/\chi_{ODT} > 3$ whereas breakout crystallization occurs with $\chi_c/\chi_{ODT} < 3$. For the blends with χ_c/χ_{ODT} around 3 the mode of crystallization is dependent on the crystallization temperature (confined at lower temperature but breakout at higher temperature). In confined crystallization the interfacial energy σ_e can be determined from crystallization rate. It is found that the values of σ_e for the E_mB_n block copolymers are slightly larger than that of PEO homopolymer. Confined crystallization can be further divided into three types based on melting behavior: partially confined crystallization for the blends with intermediate relative segregation strength having a cylinder structure in the melt, in which only part of the morphology in the melt is retained after crystallization and the other part is transformed into lamellae; "weakly" confined crystallization with no step change of q^* upon nonisothermal crystallization but remarkable change of q^* during heating for the blends with strong relative segregation strength and a cylinder structure in the melt; and "strongly" confined crystallization showing little change of q^* with temperature upon both crystallization and melting for the blends with sphere structure and strong relative segregation strength. In the range of molecular weight studied, only breakout crystallization was observed in lamellar melt morphologies.

Introduction

Recently, crystallization of block copolymers has received increasing attention due to the complex morphological changes during crystallization resulting from the competition between microphase separation and crystallization. There are usually two possibilities for the crystallization of block copolymers: confinement or breakout. In confined crystallization the morphology of the block copolymer in the melt is retained after crystallization,[1−6] whereas in breakout crystallization the morphology in the melt is destroyed upon crystallization and a lamellar structure is formed in the solid.[7−9] In glassy/crystalline block copolymers, the strong confinement of the glassy blocks can lead to crystallization confined in one, two, or three dimensions.[10] For rubber/crystalline block copolymers the situation is more complex; as well as the general behavior of confinement and breakout, other subtle morphological changes in crystallization have also been reported. Loo et al.[11] found "templated" crystallization in polyethylene-*b*-poly(styrene-*r*-ethylene-*r*-butene) (E/SEB) and polyethylene-*b*-poly(3-methyl-1-butylene) (E/MB) block copolymers, which showed the features of both confinement (such as general preservation of the cylinder structure) and breakout (for instance, sigmoid crystallization kinetics and local deformation of the morphology). Zhu et al.[12] reported a "soft" confinement on crystallization, where the block copolymer exhibited no change in domain size during crystallization but a change in domain size upon heating. Nonisothermal experiments have revealed that the crystallization of rubber/crystalline block copolymers is not only determined by segregation strength but also strongly dependent on the morphology in the melt.[13−15] Confined crystallization can be most easily observed in the sphere morphology which, for polymers with the same chain length, has a smaller segregation strength than lamellar and cylinder morphology. To understand the factors affecting the crystallization of block copolymers, Loo et al.[11] classified the crystallization of the block copolymers on the basis of the map of relative segregation strength $((\chi N_t)_c/(\chi N_t)_{ODT})$ vs volume fraction. However, because of a variety of experimental constraints, the map is incomplete, since "soft" confinement is not classified. Moreover, such a classification needs to be tested in other block copolymer systems.

In our previous work we selected different poly(oxyethylene-*b*-oxybutylene) copolymers ($\phi_B = 0.5$) with a range of chain lengths for blending with poly(oxybutylene), making a range of compositions with different

† Permanent address: Department of Polymer Science & Engineering, Zhejiang University, Hangzhou 310027, China.

‡ Present address: Polymer Science Program, Faculty of Science, Prince of Songkhla University, Songkhla 90112, Thailand.

* To whom correspondence should be addressed.

10.1021/ma0204204 CCC: $22.00
Published on Web 08/02/2002

segregation strength and morphologies using relatively few block copolymers. In the present work we report the isothermal crystallization and melting behavior of such blends. In combination with previous nonisothermal crystallization results, the features of different types of crystallization and the classification of the crystallization are reported along with a map.

Experimental Section

Materials. The synthesis and characterization of E_nB_m copolymers (where the subscripts refer to the average degree of polymerization), $E_{76}B_{38}$, $E_{114}B_{56}$, and $E_{155}B_{76}$ have been described elsewhere,[16,17] and $E_{224}B_{113}$ was prepared in a similar manner. The block copolymers have narrow molecular weight distributions ($M_w/M_n < 1.05$) measured by GPC. The PBO homopolymer with a reported $M_n \approx 2000$ g mol^{-1}(B_{28}) was purchased from Aldrich and was used without further purification. A PBO homopolymer with $M_n \approx 1000$ g mol^{-1} (B_{14}) was specially synthesized by anionic polymerization. Both have molecular weight distributions $M_w/M_n < 1.05$ by GPC.

Preparation of Blends. The blends of E_nB_m with B_h were prepared by solution blending with dichloromethane as solvent. To ensure that B_h homopolymer was miscible with B segments in block copolymers and the "wet brush" condition was met,[18,19] the molecular weight of B_h homopolymer was less than half that of the B block. As a result, $E_{76}B_{38}$ was blended with B_{14} and the other block copolymers were blended with B_{28}. Following solvent evaporation, the blends were dried under vacuum for 24 h at 60 °C and then cooled to room temperature slowly and stored below 0 °C prior to use.

Time-Resolved Small-Angle X-ray Scattering. The simultaneous time-resolved SAXS/DSC experiments were carried out on beamlines 8.2 and 2.1 of the SRS at the Daresbury, Warrington, UK. SAXS was used to monitor the change of domain size during heating after nonisothermal crystallization. The samples were cooled from the melt (lower than the order−disorder transition temperatures T_{ODT}, usually 80 °C for most of the blends, but lower temperatures for $E_{76}B_{38}$ and its blends) at a rate of 10 °C/min to complete crystallization and then were heated at rate of 10 °C/min until the order−disorder transition was observed. The data were collected in 10 s frames separated by a waiting time of 10 μs. Details of the instrument and data processing are described elsewhere.[16,17]

Isothermal Crystallization Experiments. The isothermal crystallization kinetics of the blends was carried out on a Perkin-Elmer Pyris-1 calorimeter. Samples of the copolymer (about 5−10 mg, depending on B volume fraction in the blends) were sealed with aluminum pans and were heated to the same temperature applied in SAXS experiments, held for 5 min, and then cooled at a rate of 100 °C/min to the crystallization temperatures and held until crystallization was completed. The change of heat flow with time was recorded upon crystallization. The isothermal crystallization kinetics of polymer can be analyzed using the Avrami equation:[20]

$$1 - X(t) = \frac{\Delta H^c_{t=\infty} - \Delta H^c_t}{\Delta H^c_{t=\infty} - \Delta H^c_{t=0}} = \exp(-kt^n) \qquad (1)$$

where $X(t)$ is the relative crystallinity at time t; $\Delta H^c_{t=\infty}$ and ΔH^c_t are the crystallization enthalpies on complete crystallization and after time t. Therefore, we have

$$\log[-\ln(1 - X(t))] = \log k + n \log t \qquad (2)$$

The crystallization rate constant k and Avrami exponent n can be determined from the intercept and slope in the plot of $\log[-\ln(1 - X(t))]$ vs $\log(t)$.

After isothermal crystallization, the blends were heated at a rate of 10 °C/min to 80 °C. The crystallinity (X_c) was calculated from the measured fusion heat (ΔH^E_f) using following equation:

$$X_c = \frac{\Delta H^E_f}{w_E \Delta H_f} \qquad (3)$$

where w_E and ΔH_f are the weight fraction of the E block in the blend and fusion enthalpy of perfect PEO crystals, respectively. The values of ΔH_f at different temperatures are corrected:[21−23]

$$\Delta H_f(T_1) = \Delta H_f(T_2) - 0.650(T_2 - T_1) + 0.00253(T_2^2 - T_1^2) \qquad (4)$$

where temperatures are in °C and the reference fusion enthalpy $\Delta H_f(T_2)$ is 208 J/g at 70 °C.

Table 1. Crystallization Parameters of Different Blends

sample	T_c (°C)	Avrami exponent n	log k	$t_{1/2}$ (s)	X_c
E76-83	26	2.5	−6.24	206	0.85
$E_{76}B_{38}/B_{14}$	28	2.5	−6.23	255	0.87
($\phi_B = 0.83$)	30	2.7	−6.30	306	0.89
	32	3.1	−8.06	368	0.90
E114-76	26	3.0	−5.26	49	0.80
$E_{114}B_{56}/B_{28}$	28	3.0	−6.80	162	0.82
($\phi_B = 0.76$)	30	3.1	−7.04	200	0.83
	32	3.5	−8.32	217	0.84
	−24	1.0	−2.20	104	0.72
E114-83	−23	1.2	−2.66	141	0.73
$E_{114}B_{56}/B_{28}$	−22	1.5	−3.73	196	0.77
($\phi_B = 0.83$)	−21	1.9	−4.63	252	0.79
	−20	2.5	−6.48	349	0.82
	−18	2.6	−7.33	564	0.84
E155-65	34	1.9	−3.40	76	0.82
$E_{155}B_{76}/B_{28}$	36	2.3	−4.61	97	0.84
($\phi_B = 0.65$)	38	2.3	−4.92	131	0.86
	40	2.5	−5.74	182	0.87
E155-76	−22	0.64	−1.03	41	0.73
$E_{155}B_{76}/B_{28}$	−20	0.74	−1.36	71	0.75
($\phi_B = 0.76$)	−18	0.79	−1.75	103	0.77
	−16	0.88	−2.02	138	0.79
E155-83	−24	0.95	−1.15	11	0.70
$E_{155}B_{76}/B_{28}$	−22	0.98	−1.61	31	0.72
($\phi_B = 0.83$)	−20	1.02	−2.04	70	0.74
	−18	1.05	−2.46	156	0.76
E224-76	−22	0.65	−1.16	11	0.70
$E_{224}B_{113}/B_{28}$	−20	0.73	−1.53	24	0.71
($\phi_B = 0.76$)	−18	0.78	−1.82	56	0.72
	−16	0.85	−2.18	166	0.73
E224-83	−24	0.87	−1.39	28	0.67
$E_{224}B_{113}/B_{28}$	−22	0.91	−1.79	63	0.69
($\phi_B = 0.83$)	−20	0.93	−2.25	181	0.70
	−18	1.00	−2.77	425	0.72

Results and Discussion

Isothermal Crystallization Kinetics. The Avrami exponent derived from isothermal crystallization reflects the nucleation mechanism and growth dimension of the crystals. The confined crystallization of the block copolymer is usually initiated by homogeneous nucleation and has a characteristic Avrami exponent $n = 1.0$, due to the much larger number of domains than that of heterogeneous nuclei.[12,24] In contrast, in breakout crystallization the crystals can grow in more than one dimension, and the growth of the crystals spans different domains, leading to a larger Avrami exponents ranging from 2.0 to 4.0. The Avrami exponents for the blends having sphere morphology in the melt, E76-83 ($E_{76}B_{38}/B_{14}$, $\phi_B = 0.83$), E114-83 ($E_{114}B_{56}/B_{28}$, $\phi_B = 0.83$), E155-83 ($E_{155}B_{76}/B_{28}$, $\phi_B = 0.83$), and E224-83 ($E_{224}B_{113}/B_{28}$, $\phi_B = 0.83$), are reported in Table 1. It is found that these four blends exhibit distinct crystallization behav-

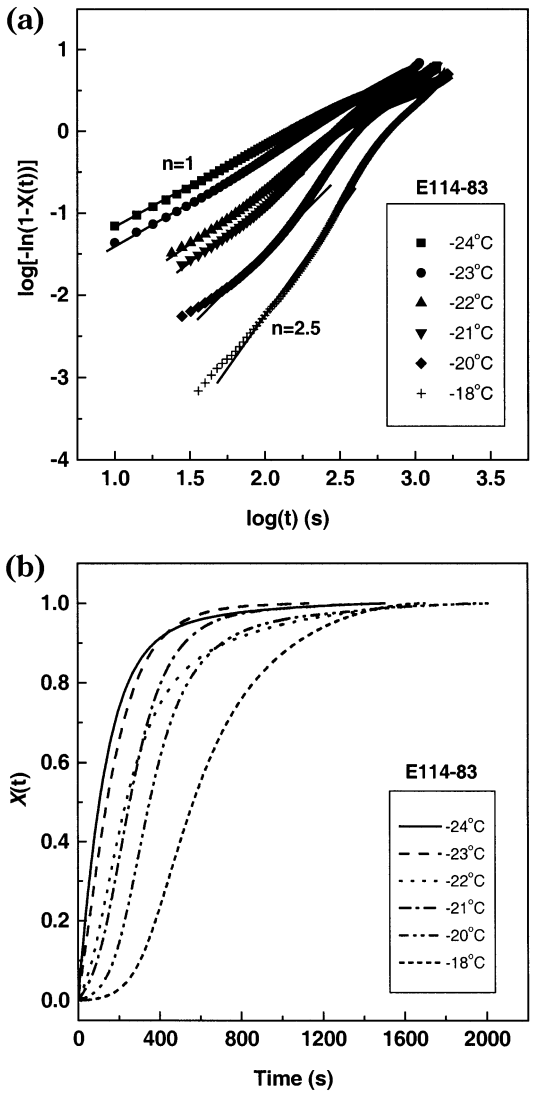

Figure 1. Avrami plots (a) and change of relative crystallinity $X(t)$ with crystallization time (b) for the blend E114-83 ($E_{114}B_{56}/B_{28}$, $\phi_B = 0.83$).

ior. The Avrami exponents of E76-83 vary from 2.5 to 3.1, which is consistent with its breakout crystallization in nonisothermal crystallization. In contrast, E114-83 exhibits a dramatic change of Avrami exponent from $n = 1.0$ at −24 °C to $n = 2.5$ at −18 °C within a narrow crystallization temperature range, as shown in Figure 1a. Figure 1b is the change of relative crystallinity $X(t)$ with crystallization time for E114-83. At lower temperature $X(t)$ rises rapidly with time at the beginning of crystallization and the crystallization curve is first order, whereas at higher temperature it is sigmoidal and there is an induction period prior to crystallization. This shows that the crystallization of E114-83 is confined at lower temperature but breaks out at higher temperature. With further increase in the chain length of the block copolymers used in the blends with $\phi_B = 0.83$, the Avrami exponents are all around 1.0 in the crystallization temperature range studied in the present work, indicating confined crystallization (see Table 1). The crystallization parameters for the blends with cylinder morphology in the melt, E114-76 ($E_{114}B_{56}/B_{28}$, $\phi_B = 0.76$), E155-76 ($E_{155}B_{76}/B_{28}$, $\phi_B = 0.76$) and E224-76 ($E_{224}B_{113}/B_{28}$, $\phi_B = 0.76$), are also reported in Table 1. The data show that E114-76 has large values of n from 3.0 to 3.5 and thus breakout crystallization, while the

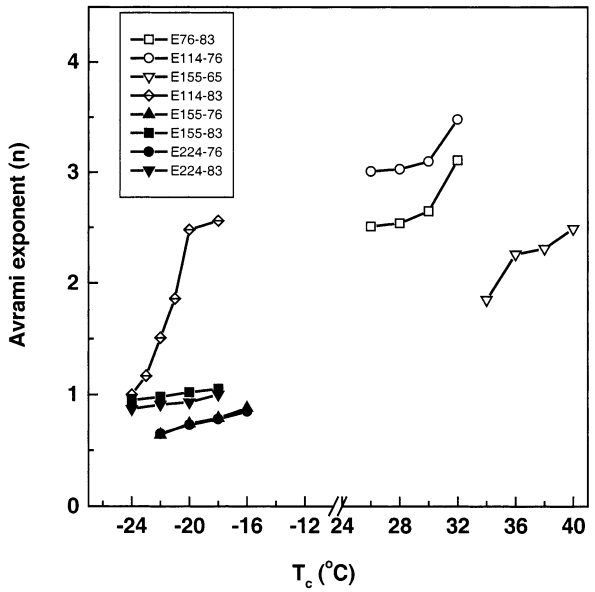

Figure 2. Plot of Avrami exponents vs composition.

other two blends E155-76 and E224-76 have Avrami exponents less than 1.0. Though the deviations of Avrami exponents from $n = 1.0$ in cylinder morphology are small, the deviations are systematic and are beyond experimental errors. Keith et al. observed an Avrami exponent of $n = 0.5$ for diffusion-controlled crystallization in the system containing high concentration of noncrystallizable impurities.[25−27] Because of the larger dimension of cylinder domains in the length direction and of the lower mobility arising from low crystallization temperature and confinement, we speculate that diffusion may also influence crystallization of PEO in a confined cylinder morphology, leading to an Avrami exponent between $n = 1.0$ and $n = 0.5$. By contrast, in sphere morphology, the size of crystal nuclei is comparable to domain size in all directions and diffusion has no influence on crystallization.

Since all of the blends with lamellar morphology, studied in the present work, undergo breakout during crystallization, only the crystallization parameters of the blend E155-65 ($E_{155}B_{76}/B_{28}$, $\phi_B = 0.65$) are exemplified in Table 1. It is observed that the Avrami exponents of this blend are between 2.0 and 2.5.

The Avrami parameters for different blends are summarized in Figure 2. It can be seen from Figure 2 that the blends can be divided into three types according to their isothermal crystallization behavior. The first type is the blends crystallizing at higher temperature, which generally have large values of Avrami exponent and the crystallization by breakout. The second type is the blends that can crystallize at lower temperature and have Avrami exponents ∼1.0. The third type shows both behaviors depending on crystallization temperature, for example E114-83, which has the Avrami exponent of confined crystallization ($n \approx 1.0$) at lower temperature but larger Avrami exponent at higher temperature. The crystallization halftimes ($t_{1/2}$) of different blends are shown in Figure 3. There is a linear relationship between $\log(t_{1/2})$ and T_c for all the blends, and the slopes are indicated in Figure 3. It is observed that the slopes for the blends with Avrami exponent $n \approx 1.0$ are remarkably larger than those with breakout crystallization. The stronger dependence of $t_{1/2}$ on T_c is another characteristic of homogeneous nucleation.[11,12,24]

Table 2. Calculated Relative Segregation Strength for the Blends with Cylinder and Sphere Morphologies in the Melt

								crystallization	
sample	ϕ_B	melt structure[a]	T_c (°C)	T_{ODT} (°C)	χ_c[b]	χ_{ODT}[b]	χ_c/χ_{ODT}	nonisothermal[15]	isothermal
$E_{76}B_{38}/B_{14}$	0.70	C	31.5	74	0.1642	0.130 4	1.26	breakout	breakout
	0.76	C	28.3	62	0.1671	0.139 0	1.20	breakout	breakout
	0.83	S	26.5	55	0.1688	0.144 4	1.17	breakout	breakout
$E_{114}B_{56}/B_{28}$	0.70	C	31.4	196	0.1643	0.067 32	2.44	breakout	breakout
	0.76	C	22.5	186	0.1726	0.071 22	2.42	confined	breakout
	0.83	S	−27.8	168	0.2310	0.078 70	2.94	confined	variable[c]
$E_{155}B_{76}/B_{28}$	0.70	C	−19.5	225	0.2198	0.056 88	3.86	confined	confined
	0.76	C	−21.5	218	0.2224	0.059 28	3.75	confined	confined
	0.83	S	−26.8	194	0.2296	0.068 09	3.37	confined	confined
$E_{224}B_{113}/B_{28}$	0.76	C	−21.0	238	0.2215	0.052 53	4.22	confined	confined
	0.83	S	−30.0	210	0.2339	0.062 07	3.77	confined	confined

[a] C stands for cylinder and S for sphere. [b] The values of χ were calculated according to eq 5. [c] Confined at lower temperature, but breakout at higher temperature.

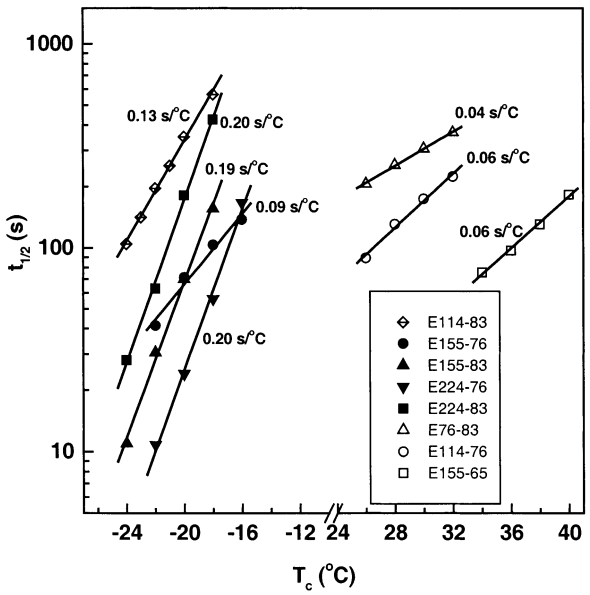

Figure 3. Crystallization halftime vs composition for different blends.

Comparing with previous results of nonisothermal crystallization,[15] we can see that most of the blends show the same crystallization behavior in both isothermal and nonisothermal experiments with the exception of E114-76 and E114-83. In nonisothermal experiments the crystallization of both E114-76 and E114-83 is confined at a cooling rate of 10 °C/min, and there is no step change in *d*-spacing as temperature decreases. Nevertheless, the isothermal crystallization kinetics reveals that breakout of crystallization occurs in E114-76 evidenced by its Avrami exponents over 3.0 and E114-83 exhibits confined crystallization at lower temperature but breakout of crystallization at a slightly higher temperature. We will address first the problem for E114-83.

The isothermal crystallization kinetics in the present work and previous nonisothermal crystallization show that strong segregation strength usually leads to confined crystallization. However, morphology in the melt also has a great influence on the crystallization behavior of the blends,[15] and this has also been observed in PEO-*b*-PB/PB blends.[13,14] For example, among the blends with lamellar, cylinder, and sphere structures in the melt, the lamellar blends have the strongest segregation strength and the sphere blends have the weakest segregation strength, but confined crystallization occurs most easily in sphere structure and we find crystallization in lamellar blends is exclusively breakout.

Loo et al.[11] used a map of volume fraction vs relative segregation strength $(\chi N_t)_c/(\chi N_t)_{ODT}$ to classify the crystallization behavior of E/SEB block copolymers finding that when the value of $(\chi N_t)_c/(\chi N_t)_{ODT}$ is below 3, the block copolymer showed breakout of crystallization; otherwise, confined crystallization was observed. The values of T_{ODT} and T_c are reported in Table 2 and have been used to estimate χ_c/χ_{ODT} from[28]

$$\chi = 84.1/T - 0.112 \tag{5}$$

Given that the samples studied here are blends of block copolymers and the noncrystalline homopolymer, reporting $(\chi N_t)_c/(\chi N_t)_{ODT}$ in a manner similar to Loo et al. is not appropriate as the factor N_t is not temperature sensitive and cancels. It is found that the blends of $E_{155}B_{76}$ and $E_{224}B_{113}$ have values of χ_c/χ_{ODT} larger than 3, in accordance with their confined crystallization behavior in isothermal crystallization. We also notice that the value of χ_c/χ_{ODT} for the blend E114-83 is 3, just near the critical value. This is the reason why the Avrami exponent of this blend is sensitive to crystallization temperature; at lower temperatures it follows first-order crystallization kinetics whereas at higher temperatures it follows sigmoidal crystallization kinetics with Avrami exponents approaching 3. The values of χ_c/χ_{ODT} for the other blends are less than 3, which is consistent with their breakout crystallization behavior.

In confined crystallization with an Avrami exponent of $n = 1.0$, crystallization is initiated by homogeneous nucleation, and the crystallization rate is determined by the rate of homogeneous nucleation. Thus, we have[29,30]

$$k \propto \exp\left[-\frac{8\pi\sigma_e^2\sigma_s(T_m^0)^2}{k_B T_c(\Delta H_f^0)^2(T_m^0 - T_c)^2\rho^2}\right] \tag{6}$$

where ΔH_f^0 and T_m^0 are the heat of fusion and the equilibrium melting temperature for infinite chain length, respectively. T_c is crystallization temperature, ρ designates the density of the crystallized E block, and k_B is the Boltzmann constant. σ_e and σ_s are the interfacial free energy between crystalline and amorphous regions for the folding surface and lateral surface of crystal nucleus.

As a result, the interfacial free energy can be derived from the slope of the plot of ln k vs $(T_m^0)^2/[T_c(T_m^0 - T_c)^2]$. Such plots for E155-76, E155-83, E224-76, and E224-83 are shown in Figure 4. The values of 208 J/g, 343 K, and 1.23 g/cm^3 are used for ΔH_f^0, T_m^0, and ρ, respectively, for all these four blends. It is found that σ_e is 43

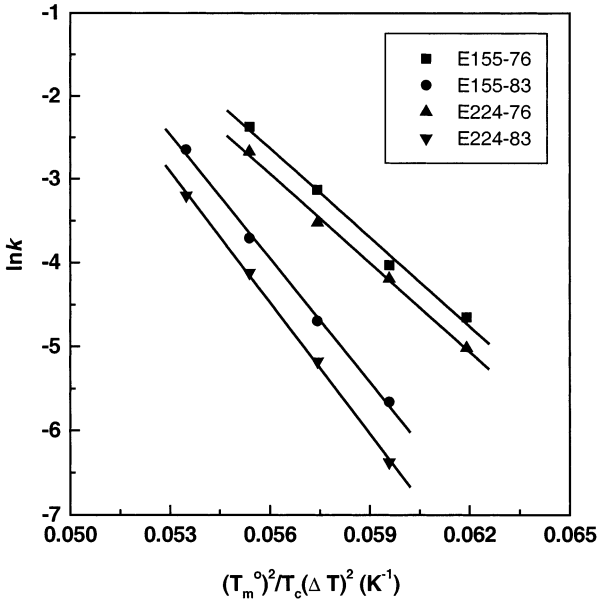

Figure 4. Plots of ln k vs $(T_m^0)^2/[T_c(T_m^0 - T_c)^2]$ for confined crystallization.

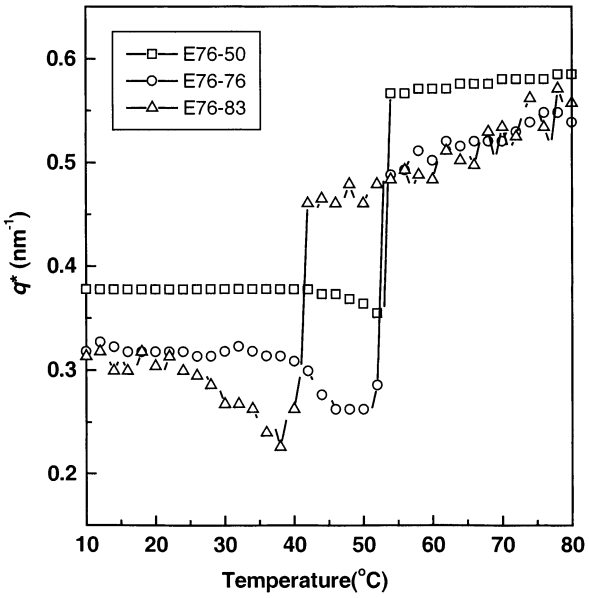

Figure 5. Change of q^* with temperature for the $E_{76}B_{38}/B_{14}$ blends during heating after nonisothermal crystallization.

mJ/m^2 for the sphere morphology and 36 mJ/m^2 for the cylinder morphology by assuming 10 mJ/m^2 for the value of σ_s.[31] These values are between those of PEO homopolymer crystals, 26 mJ/m^2 reported by Kovacs and Cheng,[32,33] and 50 mJ/m^2 (7 kJ/mol of stems and cross-sectional area is 21.4 Å^2) given by Yang,[34] which were obtained from the crystallization of PEO at higher temperature. Considering the lower crystallization temperatures in confined crystallization and the linear relationship between interfacial free energy and temperature,[35] the values of σ_e for the E_mB_n/B_h blends should be slightly larger than that of PEO homopolymer. However, when compared with the σ_e of 26 k_BT/nm^2 (91 mJ/m^2 at 253 K) in strongly segregated block copolymers poly(ethylene oxide)-*b*-polybutadiene (PEO-*b*-PB),[35] the σ_e of the E block in E_mB_n/B_h blends is relatively small. At present, we are not clear whether the smaller σ_e for cylinders results from a morphological difference or from the effect of diffusion on crystallization in cylinder domains.

Melting Behavior after Nonisothermal Crystallization. Figure 5 shows the change of q^* for some selected $E_{76}B_{38}/B_{14}$ blends during heating after nonisothermal crystallization. It is observed that there is a gradual increase of the long period (decease of q^*) during heating, followed by a step increase in q^* after complete melting. This is typical melting behavior of lamellar crystals. Figure 6 shows the SAXS profiles of E76-83. It can be seen that a lamellar structure is formed in the solid, which is supported by the second peak at $q = 2q^*$. Since the lamellar thickness distribution is inhomogeneous, the thinner crystals melt first and the thicker crystals melt last.[36] As a result, we observed that the first peak moves to lower q value during melting process. After complete melting the lamellar structure transforms into sphere morphology, and a sudden change in q^* occurs (Figure 6). The change of q^* in the melting of some $E_{114}B_{56}/B_{28}$ blends is depicted in Figure 7. It is found that the blend E114-83 shows a smooth change in q^*, in agreement with its confined crystallization during nonisothermal crystallization. The other blends, E114-50 (pure $E_{114}B_{56}$, $\phi_B = 0.50$, not shown here), E114-60 ($E_{114}B_{56}/B_{28}$, $\phi_B = 0.60$, not shown here),

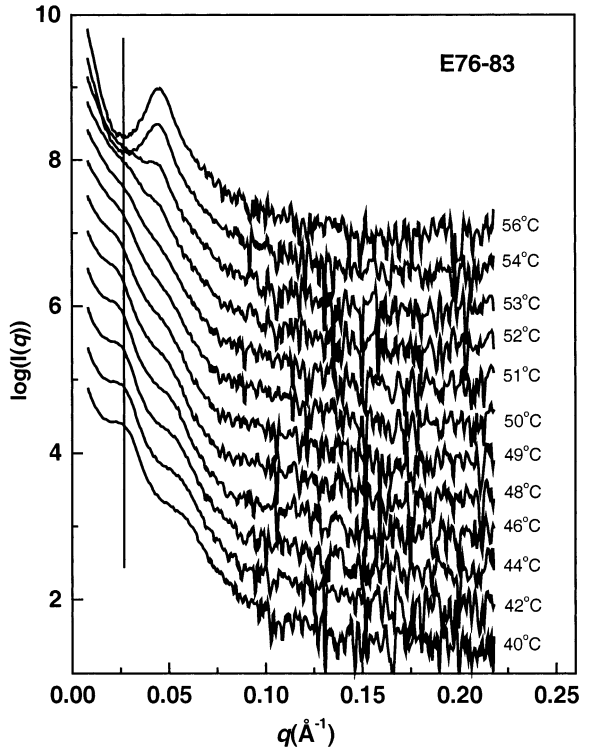

Figure 6. SAXS profiles of E76-83 ($E_{76}B_{38}/B_{14}$, $\phi_B = 0.83$) at different temperatures during heating at a rate of 10 °C/min after nonisothermal crystallization.

E114-70 ($E_{114}B_{56}/B_{28}$, $\phi_B = 0.70$), and E114-76 ($E_{114}B_{56}/B_{28}$, $\phi_B = 0.76$), exhibit a melting behavior with the characteristic of lamellar crystals, i.e., gradual decrease in q^* before melting followed by a dramatic increase. The SAXS profiles of E114-70 during heating after nonisothermal crystallization are shown in Figure 8. We can clearly see that the first-order SAXS peak in the solid of this blend indeed consists of two overlapped peaks, indicating mixed morphologies of lamellae and cylinders. This is also reflected by the broad and overlapping higher order peaks. During heating, the lowest q first-order peak moves further toward $q = 0$, suggesting that this peak corresponds to lamellar

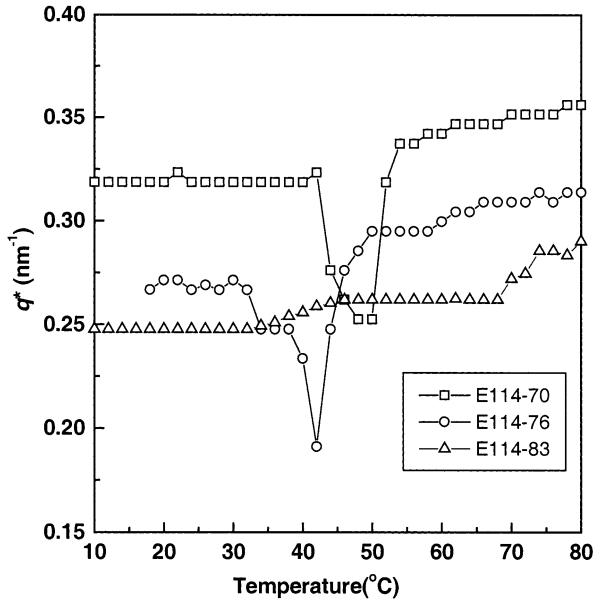

Figure 7. Variation of q^* with temperature for the $E_{114}B_{56}/B_{28}$ blends during heating after nonisothermal crystallization.

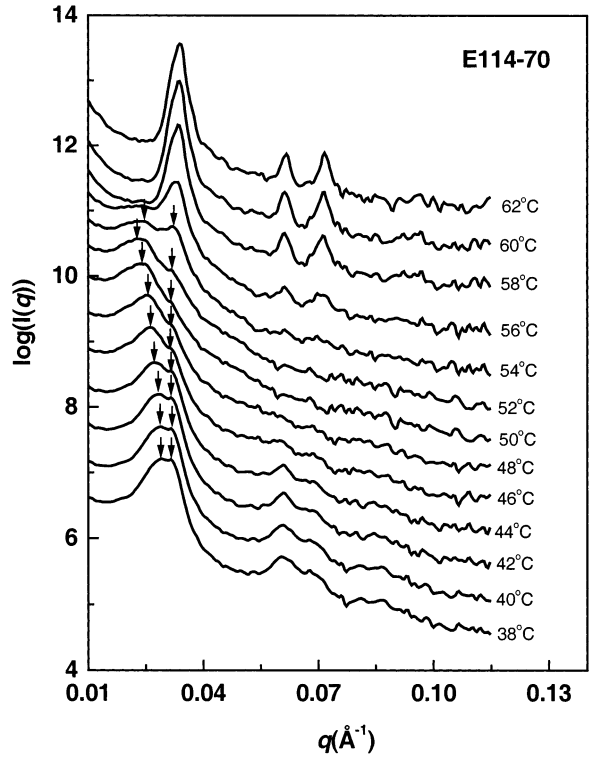

Figure 8. SAXS profiles of E114-70 ($E_{114}B_{56}/B_{28}$, $\phi_B = 0.70$) at different temperatures during heating at a rate of 10 °C/min after nonisothermal crystallization. The arrows indicate the overlapped two peaks.

structure. The higher q first-order peak, which is related to cylinder morphology, maintains its position on heating, showing that the cylinder domains are confined. E114-76 has similar SAXS profiles (not shown), but the peak corresponds to lamellar structure in the first-order peak is weaker and less obvious. Therefore, the SAXS result shows that part of cylinder morphology is still retained after nonisothermal crystallization in E114-70 and E114-76, and these two blends are partially confined. This can also explain the contradictory results of this blend in nonisothermal and isothermal crystallization. At higher temperature, the large Avrami

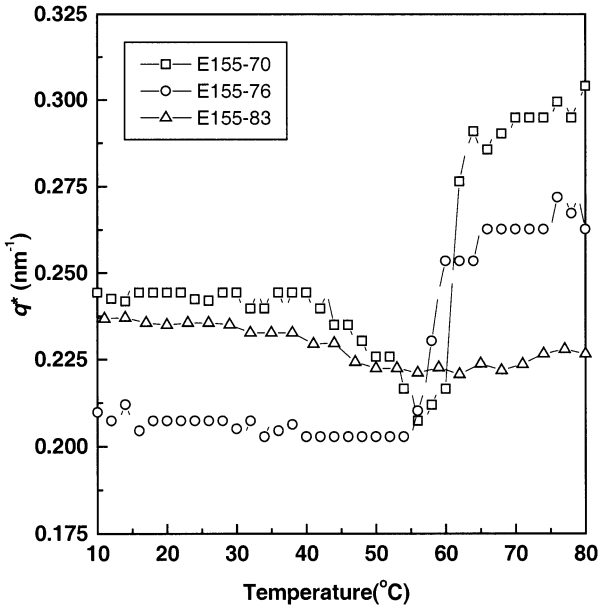

Figure 9. Variation of q^* with temperature for the $E_{155}B_{76}/B_{28}$ blends during heating after nonisothermal crystallization.

exponents reflect the breakout crystallization and the formation of lamellar crystals. In nonisothermal crystallization the fast cooling rate depresses the breakout of crystallization and confined crystallization is observed by SAXS.[15]

Figure 9 illustrates the change of q^* for some $E_{155}B_{14}/B_{28}$ blends during heating after nonisothermal crystallization. The blend E155-70 also shows a melting behavior similar to E114-70 and E114-76, indicating that the crystallization of this blend is only partially confined, and there are mixed morphologies of lamellae and cylinder in its solid. The q^* behavior of E155-83, which has a sphere structure in the melt, does not change much during melting, just like E114-83. Therefore, there is no obvious change in d-spacing upon both crystallization and melting for E114-83 and E155-83, and we classify the crystallization of these two blends as "strongly" confined. A close examination shows that the position of the first-order peak remains intact, with only the narrowing of the peak during heating (Figure 10). It is further observed that the form-factor minima of the E-spheres become more prominent as the crystals melt. The loss of form-factor minima on crystallization may be a common feature of crystallizable block copolymer systems. This results from the slight deformation of the crystalline domains upon crystallization, as has been revealed by TEM in crystalline E/SEM and E/MB block copolymers.[10,11] The broad SAXS peak in the solid is caused by the same reason. Figure 10 shows, however, that the crystalline domains remain effectively spherical as evidenced by the retention of some reduced form-factor minima in the solid. The blend E155-76 exhibits a melting behavior different from other blends. Although there is an abrupt increase in q^* after complete melting, no decrease of q^* is observed before melting. This can clearly be seen from Figure 11. The absence of the melting characteristic of lamellar crystals shows that the solid of this blend does not contain lamellar structure, and that the cylinder morphology is retained from the melt upon crystallization. Figure 12 is the change of q^* in for E155-76 a thermal cycle. We start from the melt at 80 °C and the q^* of the liquid decreases gradually during cooling before crystalliza-

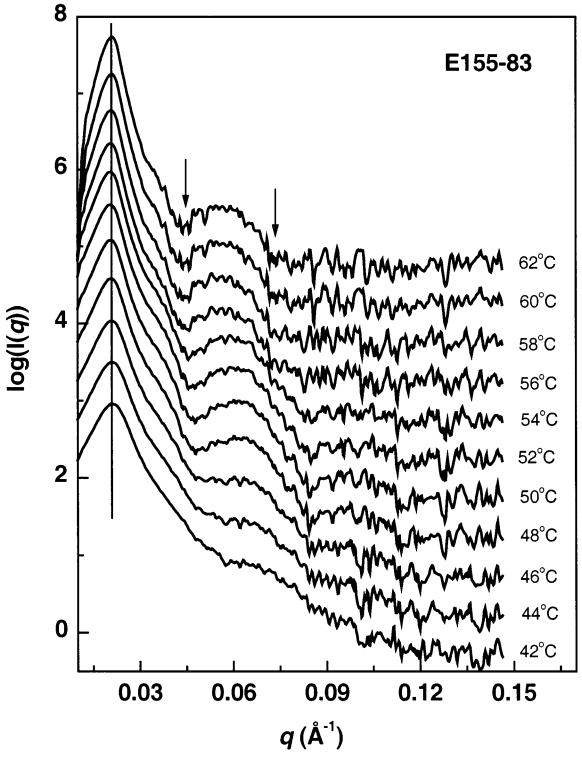

Figure 10. SAXS profiles of E114-83 ($E_{114}B_{56}/B_{28}$, $\phi_B = 0.83$) at different temperatures during heating at a rate of 10 °C/min after nonisothermal crystallization. The arrows indicate the form-factor minima.

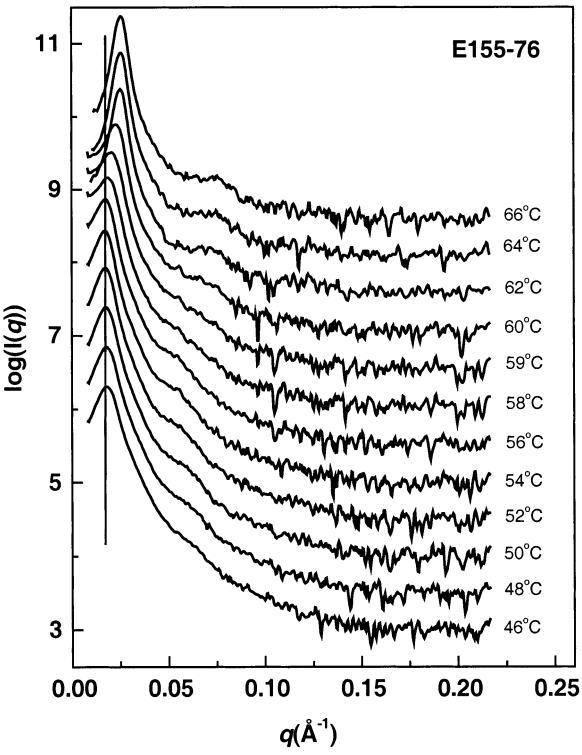

Figure 11. SAXS profiles of E155-76 ($E_{155}B_{76}/B_{28}$, $\phi_B = 0.76$) at different temperatures during heating at a rate of 10 °C/min.

tion. This is normal behavior of block copolymers as R_g increases on cooling.[37−39] This blend crystallizes at about −20 °C, and the q^* remains constant after crystallization. Then we heat the crystallized blend, and there is little change in q^* before melting. After complete melting, the blend becomes liquid again and tends to

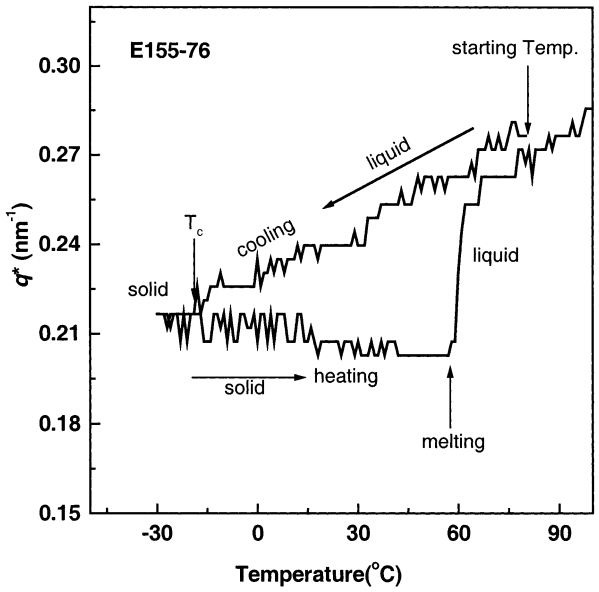

Figure 12. Variation in q^* with temperature for E155-76 ($E_{155}B_{76}/B_{28}$, $\phi_B = 0.76$) in a thermal cycle from melt to crystallization and then melting.

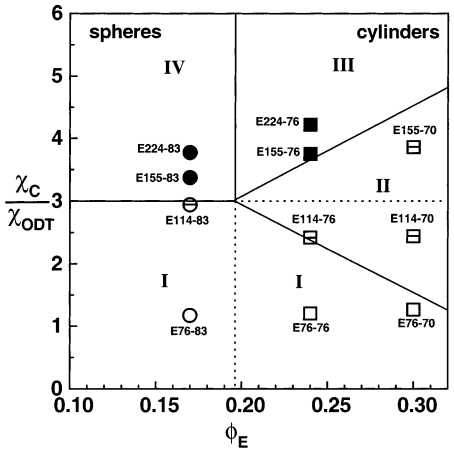

Figure 13. Classification map for the E_mB_n/B_h blends. The map is divided into four zones by the solid lines: (I) breakout zone, (II) partially confined zone, (III) weakly confined zones, (IV) strongly confined zone.

recover to the $q^*(T)$ behavior during cooling, leading to a marked increase in q^*. Therefore, we can see that the step change in q^* upon heating results from the different temperature dependence of R_g in the polymer solid and liquid. Since the domain size of E155-76 can change with temperature upon heating, we classify it as "weakly" confined. Similar "soft" confinement on crystallization was found by Zhu et al. for the blend of PEO-*b*-PS with polystyrene oligomer having a glass transition temperature (T_g) lower than crystallization temperature (T_c).[12] The blend E224-76 exhibits a melting behavior similar to E155-76 and thus is classified as "weakly" confined. For the blend E224-83 with sphere morphology, no variation in q^* is observed in the range of 0−100 °C, indicating "strong" morphological confinement.

On the basis of the results of nonisothermal crystallization, isothermal crystallization, and melting behavior, three types of confined crystallization have been identified: partial confinement, "weak" confinement, and "strong" confinement. A map of relative segregation strength vs morphology is plotted in Figure 13. We can see from the figure that the confinement and breakout

of crystallization in E_mB_n/PBO blends are well separated by the critical value of $\chi_c/\chi_{ODT} = 3$, exactly the same as in E/SEB block copolymers given by Loo et al.[11] with the triangular area of partial confinement corresponding to templated crystallization. The blends in the partial confinement area have mixed morphologies of lamellae and cylinder in their solids and exhibit a melting characteristic of lamellar crystals during heating. It should be noted that even in the partial confinement area there is some subtle differences for the blends above and blow the critical line at $\chi_c/\chi_{ODT} = 3$. For the blends above the critical line, confinement prevails over breakout and the Avrami exponent is close to 1, whereas the blends below the critical line show predominantly breakout crystallization and can crystallize at higher temperature with Avrami exponents larger than 1. Crystallization of blends in the partial confinement area, and of the blends near the critical line, is path-dependent and easily affected by crystallization conditions such as crystallization temperature in isothermal crystallization and cooling rate in nonisothermal crystallization. The areas of confined crystallization are further split into "weak" confinement area for the blends with cylinder morphology in the melt and "strong" confinement area for the blends with sphere morphology in the melt. The "weakly" and "strongly" confined blends have some common features: no step change of q^* during crystallization, Avrami exponents around 1.0, and relatively lower crystallization temperature. The difference between these two types of confined blends lies in their melting behavior. The "weakly" confined blends exhibit a step change of q^* during heating, but for the "strongly" confined crystallization the first-order peak remains constant upon melting. Since Figure 13 has great similarity to that previously reported for E/SEB and E/MB block copolymers, such a map of relative segregation strength vs volume fraction is useful for the classification of the confinement and breakout of crystallization in crystalline/rubber block copolymers and their blends. The critical value of $\chi_c/\chi_{ODT} = 3$ may be independent of the polymer chemistry; however, this needs to be tested in more systems. If this map is applicable in all systems, we can easily obtain a desired morphology by selecting suitable materials based on this map, as long as the thermodynamic parameter χ is known for the block copolymers.

Conclusions

On the basis of isothermal crystallization kinetics, the E_mB_n/B_h blends can be classified into three types: the blends crystallizing at higher temperature with large values of Avrami exponent and breakout crystallization, the blends crystallizing at lower temperature and having Avrami exponents of confined crystallization, and blends whose crystallization changes rapidly with crystallization temperature with the Avrami exponent of confined crystallization ($n \approx 1.0$) at lower temperature but larger Avrami exponent at higher temperature. The calculation of relative segregation strength χ_c/χ_{ODT} shows the isothermal crystallization of the blends is mainly determined by the segregation strength and confined or breakout crystallization can be separated by the critical line $\chi_c/\chi_{ODT} = 3$. Below this line the crystallization breaks out and above this line the crystallization is confined. The melting behavior of the blends shows that confined crystallization can be further divided into three categories: partially confined blends with mixed morphologies of lamellae and cylinder in the solid, "weakly" confined blends with no step change of q^* upon crystallization but remarkable change of q^* during heating, and "strongly" confined blends with little change of q^* in both crystallization and melting processes. This classification is exemplified using a map of relative segregation strength vs volume fraction.

Acknowledgment. J.X. was supported by The Board of Pao Yu-kong and Pao Zhao-long Scholarship and Dow Chemicals during his stay at the University of Sheffield. S.M.M. was supported by EPSRC Grants GR/L22621. Beamtime at Daresbury was provided under EPSRC Grant GR/M22116. We also thank Dr. Colin Booth for his helpful comments.

References and Notes

(1) Sakurai, K.; MacKnight, W. J.; Lohse, D. J.; Schulz, D. N.; Sissano, J. A.; Lin, J. S.; Agamalyan, M. *Polymer* **1996**, *37*, 4443.
(2) Quiram, D. J.; Register, R. A.; Marchand, G. R. *Macromolecules* **1997**, *30*, 4551.
(3) Quiram, D. J.; Register, R. A.; Marchand, G. R.; Ryan, A. J. *Macromolecules* **1997**, *30*, 8338.
(4) Rangarajan, P.; Register, R. A.; Adamson, D. H.; Fetters, L. J.; Bras, W.; Naylor, S.; Ryan, A. J. *Macromolecules* **1995**, *28*, 1422.
(5) Zhu, L.; Chen, Y.; Zhang, A. Q.; Calhoun, B. H.; Chun, M. S.; Quirk, R. P.; Cheng, S. Z. D.; Hsiao, B. S.; Yeh, F. J.; Hashimoto, T. *Phys. Rev. B: Condens. Matter* **1999**, *60*, 10022.
(6) Zhu, L.; Cheng, S. Z. D.; Calhoun, B. H.; Ge, Q.; Quirk, R. P.; Hsiao, B. S.; Yeh, F. J. *Chin. J. Polym. Sci.* **2000**, *18*, 287.
(7) Nojima, S.; Kato, K.; Yamamoto, S.; Ashida, T. *Macromolecules* **1992**, *25*, 2237.
(8) Rangarajan, P.; Register, R. A.; Fetters, L. J.; Bras, W.; Naylor, S.; Ryan, A. J. *Macromolecules* **1995**, *28*, 4932.
(9) Ryan, A. J.; Hamley, I. W.; Bras, W.; Bates, F. S. *Macromolecules* **1995**, *28*, 3860.
(10) Loo, Y. L.; Register, R. A.; Ryan, A. J.; Dee, G. T. *Macromolecules* **2001**, *34*, 8968.
(11) Loo, Y. L.; Register, R. A.; Ryan, A. J. *Macromolecules* **2002**, *35*, 2365.
(12) Zhu, L.; Mimnaugh, B. R.; Ge, Q.; Quirk, R. P.; Cheng, S. Z. D.; Thomas, E. L.; Lotz, B.; Hsiao, B. S.; Yeh, F.; Liu, L. Z. *Polymer* **2001**, *42*, 9121.
(13) Chen, H. L.; Wu, J. C.; Lin, T. L.; Lin, J. S. *Macromolecules* **2001**, *34*, 6936.
(14) Chen, H. L.; Hsiao, S. C.; Lin, T. L.; Yamauchi, K.; Hasegawa, H.; Hashimoto, T. *Macromolecules* **2001**, *34*, 671.
(15) Xu, J. T.; Turner, S. C.; Fairclough, J. P. A.; Mai, S. M.; Ryan, A. J.; Chaibundit, C.; Booth, C. *Macromolecules* **2002**, *35*, 3614.
(16) Mai, S. M.; Fairclough, J. P. A.; Terrill, N. J.; Turner, S. C.; Hamley, I. W.; Matsen, M. W.; Ryan, A. J.; Booth, C. *Macromolecules* **1998**, *31*, 8110.
(17) Mai, S. M.; Fairclough, J. P. A.; Viras, K.; Gorry, P. A.; Hamley, I. W.; Ryan, A. J.; Booth, C. *Macromolecules* **1997**, *30*, 8392.
(18) Tanaka, H.; Hasegawa, H.; Hashimoto, T. *Macromolecules* **1991**, *24*, 240.
(19) Winey, K. I.; Thomas, E. L.; Fetters, L. J. *Macromolecules* **1992**, *25*, 2645.
(20) Avrami, M. *J. Chem. Phys.* **1939**, *7*, 1103.
(21) Campbell, C.; Viras, K.; Richardson, M. J.; Masters, A. J.; Booth, C. *Makromol. Chem.* **1993**, *194*, 799.
(22) Yang, Z.; Yu, G. E.; Cooke, J.; Ali-Adib, Z.; Viras, K.; Matsuura, H.; Ryan, A. J.; Booth, C. *J. Chem. Soc., Faraday Trans.* **1996**, *92*, 3173.
(23) Cooke, J.; Viras, K.; Yu, G. E.; Sun, T.; Yonemitsu, T.; Ryan, A. J.; Price, C.; Booth, C. *Macromolecules* **1998**, *31*, 3030.
(24) Loo, Y. L.; Register, R. A.; Ryan, A. J. *Phys. Rev. Lett.* **2000**, *84*, 4120.
(25) Keith, H. D.; Padden, F. J. *J. Appl. Phys.* **1964**, *35*, 1286.
(26) Keith, H. D.; Padden, F. J. *J. Appl. Phys.* **1964**, *35*, 1270.
(27) Sperling, L. H. *Introduction to Physical Polymer Science*, 2nd ed.; John Wiley & Sons: New York, 1992; p 234.
(28) Ryan, A. J.; Mai, S. M.; Fairclough, J. P. A.; Hamley, I. W.; Booth, C. *Phys. Chem. Chem. Phys.* **2001**, *3*, 2961.

(29) Uhlmann, D. R.; Kritchevsky, G.; Straff, R.; Scherer, G. *J. Chem. Phys.* **1975**, *62*, 12.
(30) Wunderlich, B. *Macromolecular Physics;* Academic Press: London, 1976; Vol. 2.
(31) Richardson, P. H.; Richards, R. W.; Blundell, D. J.; Macdonald, W. A.; Mills, P. *Polymer* **1995**, *36*, 3059.
(32) Kovacs, A. J.; Gonithier, A. *Kolloid Z. Z. Polym.* **1972**, *250*, 530.
(33) Cheng, S. Z. D.; Chen, J. H.; Janimak, J. J. *Polymer* **1990**, *31*, 1018.
(34) Yang, Z.; Cooke, J.; Viras, K.; Gorry, P. A.; Ryan, A. J.; Booth, C. *J. Chem. Soc., Faraday Trans.* **1997**, *93*, 4033.
(35) Hong, S.; Yang, L. Z.; MacKnight, W. J.; Gido, S. P. *Macromolecules* **2001**, *34*, 7009.
(36) Ryan, A. J.; Stanford, J. L.; Bras, W.; Nye, T. M. W. *Polymer* **1997**, *38*, 759.
(37) Mai, S. M.; Fairclough, J. P. A.; Hamley, I. W.; Matsen, M. W.; Denny, R. C.; Liao, B. X.; Booth, C.; Ryan, A. J. *Macromolecules* **1996**, *29*, 6212.
(38) Wolff, T.; Burger, C.; Ruland, W. *Macromolecules* **1993**, *26*, 1707.
(39) Sakamoto, N.; Hashimoto, T. *Macromolecules* **1995**, *28*, 6825.

MA0204204